Digital Discovery

ROYAL SOCIETY OF CHEMISTRY

PAPER

View Article Online
View Journal | View Issue

Cite this: *Digital Discovery*, 2024, **3**, 1430

High throughput methodology for investigating green hydrogen generating processes using colorimetric detection films and machine vision†

Savannah Talledo, Andrew Kubaney, Mitchell A. Baumer, Keegan Pietrak and Stefan Bernhard *

The generation of hydrogen from abundant and renewable precursors driven by sunlight will be a cornerstone of a future, sustainable hydrogen infrastructure. Current methods to monitor the evolution of hydrogen in such photocatalytic systems such as gas chromatography, mass spectrometry, manometry or Raman spectroscopy are either expensive and low throughput or lack sensitivity and selectivity over other gasses. These impediments hinder the generation of photo-driven hydrogen evolution data necessary for machine learning and artificial intelligence-based protocols. This work presents an open-source approach for studying solar-driven hydrogen evolution reactions (HERs) in parallel that uses colorimetric hydrogen detection films in tandem with an image analysis software capable of providing metrics such as hydrogen amount, hydrogen evolution rates, incubation times, and plateau times. The sensing medium is composed of 0.05% (w/w) Pt impregnated molybdenum(VI) oxide or tungsten(VI) oxide which was incorporated into poly(vinyl alcohol) films placed under clear, gas impermeable septa. To conduct experiments, users require only blue reaction-driving high intensity LEDs (light emitting diodes), a camera, and uniform lighting to take pictures as the septa darken. This work introduces a sample configuration in which nine samples in hydrogen sensitive septa-capped vials were illuminated and the gas evolution is monitored using a RaspberryPi for image capture and storage. Two calibration methods are presented, one uses a gravimetric hydrogen evolution with Zn/HCl that is compared to a direct hydrogen injection. Both methods allow the accurate correlation of normalized intensity values of film photographs to mole fractions of H_2 ranging from 0 to 50%. Four light-driven HERs are described that highlight the capabilities of the detection method, two of which were conducted using the novel septa-based instrumentation while the other two experiments used the films on a 108 multiwell plate using a previously described photoreactor.

Received 7th March 2024
Accepted 10th June 2024

DOI: 10.1039/d4dd00070f

rsc.li/digitaldiscovery

1 Introduction

Finding alternative energy sources to replace fossil fuels and keep up with increasing energy demands has been a topic of immense interest for decades. Hydrogen is a promising green fuel due to its high energy density and water being the only byproduct upon oxidation; however, at present hydrogen is sourced predominantly from steam-methane reforming which generates 7.5 to 12 tons of CO_2 per ton of H_2.[1,2] In an effort to avoid harmful emissions, solar-driven hydrogen evolution is being explored as an alternative. Such light-driven hydrogen evolving reactions (HERs) use the energy of photons *via* a light absorbing chromophore to reduce water or protons in solution to afford H_2. This is commonly explored using three component systems consisting of a photocatalyst (PC), electron donor (D), and water reduction catalyst (WRC) (see Fig. 1).[3–5] When the photocatalyst is irradiated, it can enter an excited state which can be reductively quenched by the D *via* a single electron transfer. The oxidation of the donor generates a reduced PC species that can transfer an electron to the WRC, regenerating the ground state PC. Water or protons in solution can be reduced by the WRC^-, evolving H_2. Donors are very commonly sacrificial in nature such as ascorbic acid[6,7] and tertiary amines,[8,9] but it is desirable to transition to bioavailable reagents[10,11] or water.[12,13] Reagents such as oxalic acid or isopropanol are thought to proceed *via* an oxidative quenching pathway (see Fig. 1B) which begins with the irradiation of the PC, generating the excited state PC*. This species is responsible

Department of Chemistry, Carnegie Mellon University, 4400 Fifth Avenue, Pittsburgh, Pennsylvania 15213, USA. E-mail: bern@cmu.edu; Tel: +1-(412) 268-7419

† Electronic supplementary information (ESI) available: This section includes a labeled image of the RaspberryPi and relay board wiring configuration for the 20 mL vial photoreactor and the calibration curve used for the analysis of the multiwell plate experiments (PDF). It also includes the processed image analysis data and a movie of the reaction progress from Experiment 2, information on making a mask, image analysis Python script, photoreactor Python script, and sample holder STL file for 3D printing (ZIP files). See DOI: https://doi.org/10.1039/d4dd00070f

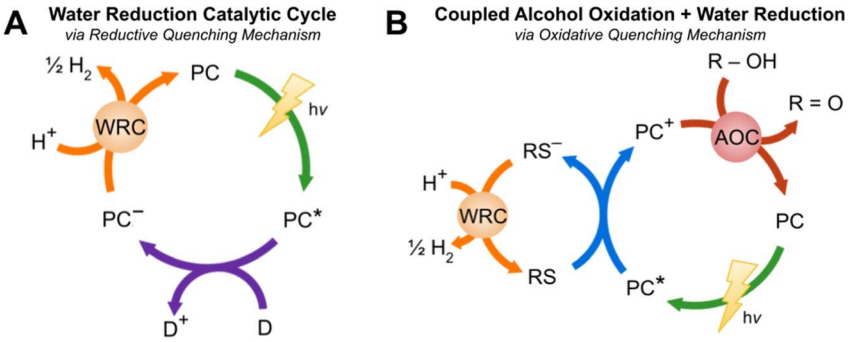

Fig. 1 (A) Light-driven water reduction catalytic cycle[14] for the photogeneration of H_2 proceeding *via* a reductive quenching mechanism composed of a PC, D, and WRC. (B). Photo-driven coupled alcohol oxidation and water reduction catalytic cycle[14] *via* an oxidative quenching mechanism containing a PC, RS, WRC, AOC, and R–OH.

for the reduction of a redox shuttle (RS) which is able to reduce the WRC. The ground state PC is regenerated *via* the oxidation of the OH-functionalized donor, a process that may be assisted by an alcohol oxidation catalyst (AOC). Oxidation of the donor generates protons in solution that can be reduced by the WRC to afford H_2. Due to the complexity of these systems, no sustainable alternative for hydrogen production has been discovered; therefore, more powerful research methods that will allow for a greater understanding of such light to chemical energy transformations is urgently required.

One way to improve these photocatalytic systems is by creating an accessible tool that can accurately and efficiently monitor hydrogen evolution reactions in high-throughput, which could provide the data necessary for building insightful artificial intelligence-based tools or machine learning models. Unfortunately, introducing light-driven HERs to these environments can pose many challenges as the predominant tool used to monitor hydrogen evolution, gas chromatography, is expensive, requires hydrogen gas as a standard, and experiments can only be conducted in low throughput.[15] Alternative approaches using headspace Raman spectroscopy or mass spectrometry are facing similar obstacles.[16] Inexpensive and accessible solutions such as the use of pressure transducers or hydrogen sensors have been used, but often lack accuracy and selectivity for hydrogen over other potential gasses that may evolve in HERs such as CO, CO_2, and O_2.[17–19] While some efforts towards developing high-throughput techniques for the synthesis of photocatalysts and studying light-driven HERs have been made,[20,21] the instrumentation and characterization methods employed are costly and thus impractical for widespread use.

This work offers an inexpensive, open source, research grade method to study light-driven HERs by utilizing colorimetric hydrogen detection films, a photoreactor built using readily available materials, and an image analysis code written in Python. The films are made of poly(vinyl alcohol) (PVA) and contain 0.05% (w/w) Pt impregnated molybdenum(VI) oxide or tungsten(VI) oxide as the hydrogen sensing material. Detection of hydrogen using this material is achieved by the hydrogen spillover mechanism, a process previously studied by Adams and Chen.[22] Hydrogen atoms dissociate onto the surface of the platinum catalyst and are able to migrate and diffuse into the metal oxide (MO_3) (Fig. 2). The introduction of hydrogen radicals into the metal oxide allows for the formation of deep blue tungsten/molybdenum bronze (H_xMO_3).[23] This color change can be attributed to the generation

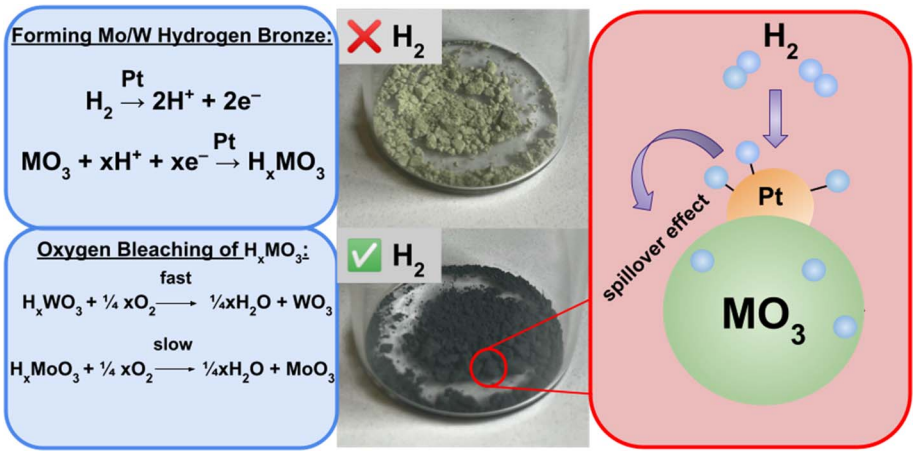

Fig. 2 Platinum catalyzed reduction of a metal oxide (M = tungsten or molybdenum) to form deep blue colored tungsten/molybdenum bronze (H_xMO_3) and its much slower reverse reaction (left). Images of the hydrogen sensing material in the presence and absence of H_2 (middle). Depiction of the dissociation of H_2 on the surface of the platinum catalyst and subsequent spillover of hydrogen atoms into the metal oxide lattice (right).

of M^{5+}, creating a mixture of the metal occupying oxidation states of 5+ and 6+, allowing for intervalence charge transfers (IVCT) to occur in the visible region.[24,25]

When selecting a sensing material to study a hydrogen evolving system, it is important to consider the experiment duration, predicted amount of H_2 generated and other factors as one metal oxide may be preferred over another. The tungsten bronze sensing material has wider limits of detection and a quicker reverse reaction, while the molybdenum bronze is more sensitive to smaller changes in H_2 evolution, surveys a smaller range of H_2 concentration, and exhibits an extremely slow reverse reaction.[26] These colorimetric H_2 detection films can be implemented in a variety of relevant configurations, with applications that include (photo)-electrochemical cells, multiwell plates, and flow cells. In this manuscript, two configurations suited for colorimetric detection are discussed; the first of which has been reported previously[27] with a once commercially available H_2 detection tape on a 96 multiwell plate. Additionally, a novel, more accessible approach is presented where the H_2 sensing films have been placed under clear, gas impermeable septa fitted for 20 mL screw cap vials. A photoreactor composed of blue and white strip LEDs, camera, and stir plate are able to house nine sample vials to study light-driven HERs. A RaspberryPi single board computer stores and executes a program written in Python that controls the illumination of the samples and times the digital imagery of the films to monitor reaction progress. Two calibration methods are presented, one uses H_2 gas as a standard while the second technique employs a gravimetric method that utilizes the dissolution of zinc in acid. An image analysis program written in Python is used to generate calibration curves correlating the normalized darkness from the images of the films throughout an experiment to a mole fraction of evolved H_2. Four light-driven HER chemistries have been described here to show a selection of experiments users could use as standards or expand upon in a research setting. Experiment 1 demonstrates how the detection films can be used to survey the chemical space of a solar H_2 evolution system composed of earth abundant reagents. Experiment 2 uses a parallelized synthetic technique to generate 96 unique iridium photosensitizers on a multiwell plate to explore structure–activity relationships between photocatalyst identity and H_2 production. Experiment 3 involves different mono and bimetallic *in situ* generated nanoparticulate WRCs to illustrate how the sensing technology can uncover synergistic effects in H_2 activity. While Experiments 1, 2, and 3 use tertiary amines as sacrificial electron donors, Experiment 4 surveys eight different bioavailable donors at varying reaction conditions on a multiwell plate and compares their efficiencies for photo-generating H_2. It is the desired outcome of this work that researchers are provided an accessible and effective method of studying solar-driven H_2 evolution systems for the development of predictive models for the discovery of novel photocatalytic HERs.

2 Experimental

2.1 Fabrication of hydrogen detection films

2.1.1 Formulation of hydrogen sensing material. The synthetic procedure was adapted from previous publications.[28,29] 5 mg of potassium tetrachloroplatinate was added to a 100 mL aqueous suspension containing 10 g of either molybdenum(VI) oxide or tungsten(VI) oxide. This mixture was vigorously stirred at room temperature for two hours. Sodium hydroxide (2.5 g for WO_3 and 225 mg for MoO_3) and sodium borohydride (500 mg for WO_3 and 30 mg for MoO_3) were added and the mixture was stirred for 2 hours at room temperature. The resulting powder was filtered, washed with water (2 × 10 mL), and dried under vacuum.

2.1.2 Suspension of sensing material into films. Films were made using poly(vinyl alcohol) (PVA, 87–90% hydrolyzed, average mol wt 30 000–70 000) using a protocol for formulating the polymer solution adapted from previously published work.[30] For ease of preparation, the following process could be done in tandem with the powder formulation described above. A 500 mL round bottom flask containing 285 mL of water was heated to 35 °C. 15 g of PVA was added and fully dissolved with stirring before heating to 85 °C using a reflux condenser for three hours. The resulting mixture was cooled to room temperature and covered. 360 mg of the tungsten containing or 600 mg of the molybdenum containing hydrogen sensing powder were placed in a 40 mL vial with a minimal amount (2–3 mL) of water and agitated until no clumps remained. 25 g of the PVA solution was poured into the same vial, stirred vigorously for several minutes, and quickly poured into a plastic Petri dish with a 150 mm diameter. The films were cured at room temperature overnight. Film thickness was measured using a digital micrometer and was found to be 40–50 microns when measured at four random points on the film across four different films. Films were stored in reclosable plastic bags until they were ready to be used.

2.1.3 Incorporation of hydrogen detection films into septa. The septa were designed to replace those found in commercially available EPA vials (see Fig. 3). A thin layer of 0.005″ clear moisture-resistant polyester film (McMaster-Carr 8567K52) was adhered to 0.06″ clear high-purity high-temperature silicone rubber strip (McMaster-Carr 5542N136) using double sided Scotch™ tape. 0.0035″ fluorinated ethylene propylene (FEP) plastic film (McMaster-Carr 5805T11) with its own adhesive backing was placed on the opposite side of the silicone. Lastly, the H_2 detection film was adhered underneath the FEP using double sided Scotch™ tape. The septa were cut to the appropriate size using a 7/8″ hammer-driven hole punch (McMaster-Carr 3427A22). Having a layer of opaque, thin H_2 permeable silicone under the detection film may be required with samples that use highly volatile solvents or operate under harsher conditions.

2.2 Instrument design

2.2.1 Hardware and control. The photoreactor shown on the left in Fig. 4 was built using an inexpensive, single-board, control computer and readily available materials. This work utilizes automated instrumentation for monitoring the colorimetric film response, but experiments can be conducted with the detection films as long as the user has access to a camera, uniform lighting, and high intensity LEDs. This sample set up

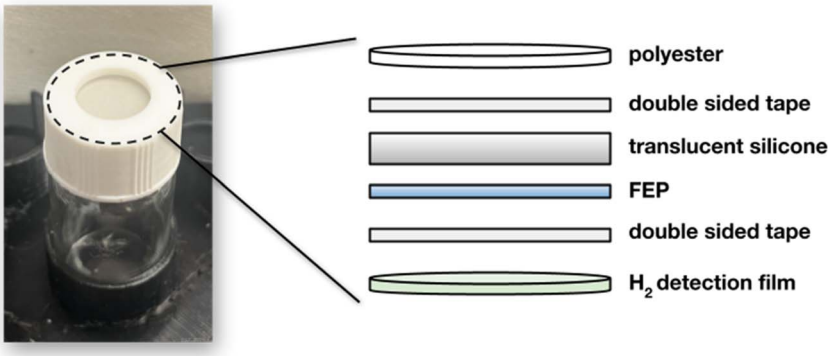

Fig. 3 Image of an assembled gas tight septum and a visual representation of its assembled materials from top to bottom consisting of polystyrene, double sided tape, translucent silicone, FEP, double sided tape, a H_2 detection film.

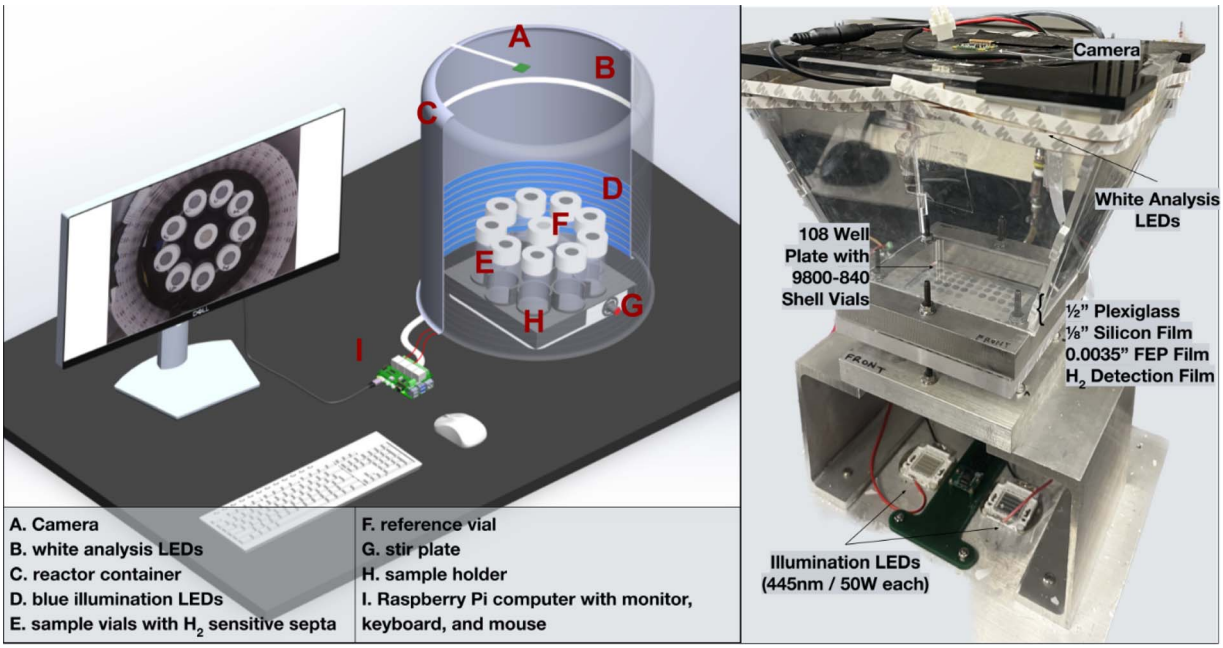

Fig. 4 Visual rendering of H_2 evolution photoreactor and its labeled parts (left). A picture of the wiring of the reactor set up can be found in the ESI (Fig. S1†). Labeled image of a multiwell plate hydrogen evolution photoreactor (right). Design files for this setup can be found in a previous publication.[31]

includes nine 20 mL EPA vials charged with stir bars and capped with hydrogen sensing septa, which were placed inside a 3D printed sample holder made of polylactic acid (PLA) with an additional empty reference vial placed in the center. The sample holder was designed to fit atop a stir plate (see ESI† for CAD File). A reactor container (8″ duct galvanized steel adjustment sleeve, McMaster-Carr 1761K127) containing blue illumination strip LEDs and white analysis strip LEDs was placed around the vials and a lid made of 0.25″ acrylic with a RaspberryPi CameraV2 mounted in the center was used to cover the container. The photoreactors' lights are controlled by a RaspberryPi computer that also captures and stores the pictures documenting the septa's color changes. The photoreactor shown on the right in Fig. 4 is capable of housing a 108 multiwell plate whose components were discussed at length in a previous publication.[27]

Experiments from both reactors shown in Fig. 4 are controlled with a program written in Python that can be found in the ESI.† A block diagram outlining the operations that occur when executing the photoreactor code has been provided in Fig. 5. Input parameters include the experiment duration and the time intervals at which pictures are taken in minutes. Each experiment begins with an initial image of the films. The vials are illuminated with blue LEDs for the desired experiment length with pauses at distinct intervals where pictures are taken with white light. The timing of the lighting is controlled by a 5 V relay board interfaced to the Raspberry Pi's GPIO interface (see ESI† for wiring details).

2.2.2 Image analysis software. After an experiment is complete, images are read through a Python script that can also be found in the ESI.† A flowchart describing the steps involved in the image analysis code are provided in Fig. 6. In order for the

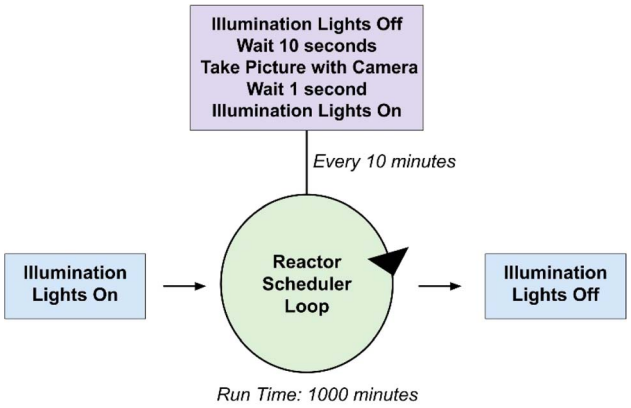

Fig. 5 Block diagram detailing the flow of commands for the H_2 evolution photoreactor code.

code to identify each individual sample, a mask using the first image is made in a free and open-source raster graphics editor, such as GIMP (see ESI†). The program monitors the change in the averaged RGB (red, green and blue) values of each individual sample and undergoes two normalizations to cancel the effects of fluctuations caused by the lighting source and the camera. First, each sample in every image is normalized by the reference vial for that specific image. This removes any changes in the signal intensities that may have occurred from image to image that are not due to H_2 evolution. Then, the average RGB values of every sample in every image is normalized by the intensity of that sample's first image.

Changes in sample RGB intensity can be correlated to a mole fraction of H_2 evolved once calibrated. Data is exported as a CSV file and contains the normalized raw reference intensity (the intensity value of the reference normalized by the first image, this value should be 1 for the first image and should only change slightly throughout an experiment), normalized reference intensity (the intensity value of the reference normalized by the first image and by the reference well, this value should always be 1), normalized sample intensity (the averaged RGB values for each sample in every image), H_2 mole fraction, H_2 volume, H_2 amount, and H_2 rate at every time point. It also outputs the maximum H_2 amount, maximum H_2 rate, H_2 incubation time (time before any H_2 is generated), and H_2 plateau time (time H_2 evolution halts) for each sample. It is important to note that the image analysis can also be performed manually with any image processing software that allows access to RGB values of pixels.

2.3 Film calibration

There is great flexibility in how the H_2 detection films can be calibrated. The process by which the films were calibrated on the multiwell plate photoreactor has been discussed previously[27] and the corresponding calibration curve can be found in the ESI (Fig. S2).† This work presents two methods to survey the analytical signal and the limits of detection of the films for the 20 mL vial photoreactor configuration. Images of the films with no H_2 present and pictures showing the films after they have responded were read through the image analysis software described previously to obtain the intensity values of the films for different amounts of H_2. Calibration curves were made by plotting intensity *vs.* mole fraction of H_2 which produce a linear relationship with good R^2 values and almost identical results for both calibration methods. Their calibration equations can be implemented into the image analysis program to correlate changes in intensity of the films to a quantitative amount of H_2.

2.3.1 Calibration method A: gravimetric. The following calibration option utilizes the reaction $Zn(s) + HCl(aq) \rightarrow H_2(g) + ZnCl_2$ in which nine different masses of zinc dust (<150 μm) were weighed in triplicate to evolve stoichiometric amounts of H_2 that span mole fractions between 0–0.5. After the initial picture was taken, 2 mL of a 2 M HCl solution and 2 mL of 2-methoxyethanol were added to every vial. The samples were immediately capped and stirred for thirty minutes. Another picture was taken of the samples showing the range of response (Fig. 7).

2.3.2 Calibration method B: hydrogen gas injection. This calibration method requires H_2 gas and a gas-tight syringe. An initial picture of nine vials capped with septa containing the H_2 detection films containing no H_2 was taken. A known volume of atmospheric H_2 was injected into all nine vials through the septa and given thirty minutes to respond, after which an image was acquired. This process was repeated for a total of nine injections that increased the H_2 mole fractions from 0 to 0.5

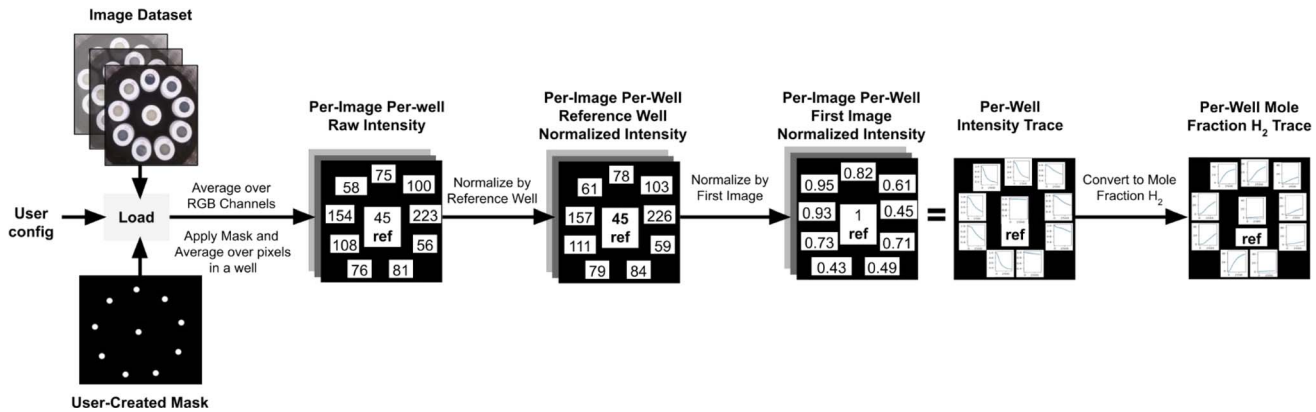

Fig. 6 Block diagram detailing the flow of commands for the H_2 evolution photoreactor code.

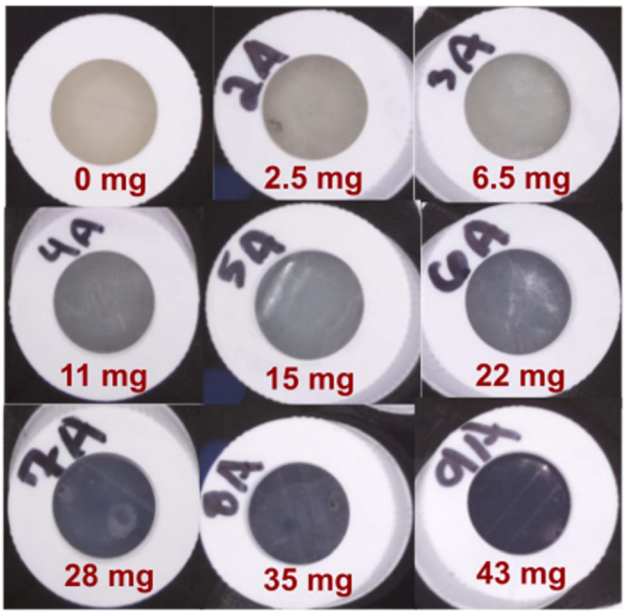

Fig. 7 Colorimetric response of tungsten oxide-based films for nine different zinc masses dissolved in HCl.

gradually (Fig. 8). Mole fractions were calculated by converting the volume injected to moles of H_2 using the ideal gas law and dividing by the sum of the moles of air in the vial's headspace and moles of H_2.

2.4 Chemistries: materials and methods

Four HER experiments have been performed using the H_2 detection films as a means of demonstrating the range of the sensing technology. Experiments 1 and 3 were conducted using the tungsten oxide-based films placed under translucent septa fitted for 20 mL scintillation vials and Experiments 2 and 4 were performed using the molybdenum oxide films sealed on multiwell plates.

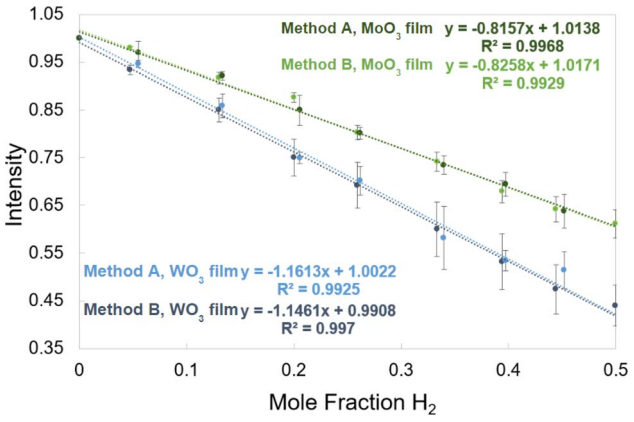

Fig. 8 Calibration curves for the W and Mo containing hydrogen detection films using both calibration methods. Normalized intensity values of the images are plotted against the mole fraction of hydrogen injected or evolved in the wells.

2.4.1 Experiment 1: organic dyes and earth abundant water reduction catalysts. There is an effort to have H_2 evolution systems operate using inexpensive and earth abundant materials to increase the probability of a successful implementation of the technology in an industrial setting. This can be achieved using organic dyes as photocatalysts[32,33] and first row transition metal containing water reduction catalysts.[34,35] Experiment 1 explores the chemical space of one of these systems previously studied,[36] and is proposed to proceed mechanistically as described in Fig. 1. The system is composed of the organic dye Eosin Y as the PC, triethanolamine (TEOA) as the D, and chloro (pyridine)cobaloxime(III) as the WRC.

All of the materials used in this system are commercially available, though chloro (pyridine)cobaloxime(III) was synthesized according to literature,[37] but can be purchased from Sigma Aldrich. Stock solutions of the PC and WRC were made in 2-methoxyethanol. TEOA was made as a 60% (w/w) solution in deionized water. Nine solutions spanning three different WRC (0.25, 0.5, 1 mM) and PC (0.5, 1, 2 mM) concentrations were made, all of which contained 0.8 mL of the TEOA stock and 7.2 mL of methoxyethanol. These solutions are stable for weeks and be used as internal standards in septum-based and multiwell plate experiments. Images of the films were taken every 10 minutes for a total duration of 1000 minutes of illumination; however, experiments do not require this entire duration to exhibit a range of response in the films.

2.4.2 Experiment 2: structure–activity relationships with 96 unique photocatalysts. Experiment 2 is designed to exhibit the H_2 detection films compatibility with high-throughput synthetic techniques that allows the rapid generation of a large H_2 evolution dataset, that can aid in elucidating structure–activity relationships between a photocatalyst identity and the H_2 it evolved. This is demonstrated by using heteroleptic iridium(III) complexes containing two cyclometallating (C^N) ligands and one ancillary (N^N) ligand with varying substituents (Fig. 9) as PCs. This experiment surveys the H_2 activity of 96 combinatorially synthesized photosensitizers in a three-component water reduction system in which TEOA was the donor and *in situ* generated palladium nanoparticles acted as the WRC.

Fig. 9 outlines twelve different cyclometallating ligands (C^N) and eight different ancillary (N^N) ligands that were used to synthesize 96 unique iridium(III) photosensitizer in 1.1 mL shell vials. All complexes contain a Cl^- counterion. Experimental conditions for the parallelized synthesis were derived from previously published work.[38] 150 microliters of an aqueous stock solution composed of 30% (w/w) TEOA and 0.65 mM potassium tetrachloropalladate (K_2PdCl_4) were added to all 96 wells. The samples were sealed with a hydrogen detection film using torqued screws to produce a uniform pressure. The samples were then illuminated for 1000 minutes using the multiwell plate H_2 evolution photoreactor, and images of the films were taken every ten minutes.

2.4.3 Experiment 3: mono and bimetallic water reduction catalysts. Noble metals such as palladium and platinum are known to be efficient WRCs, but as these metals are expensive

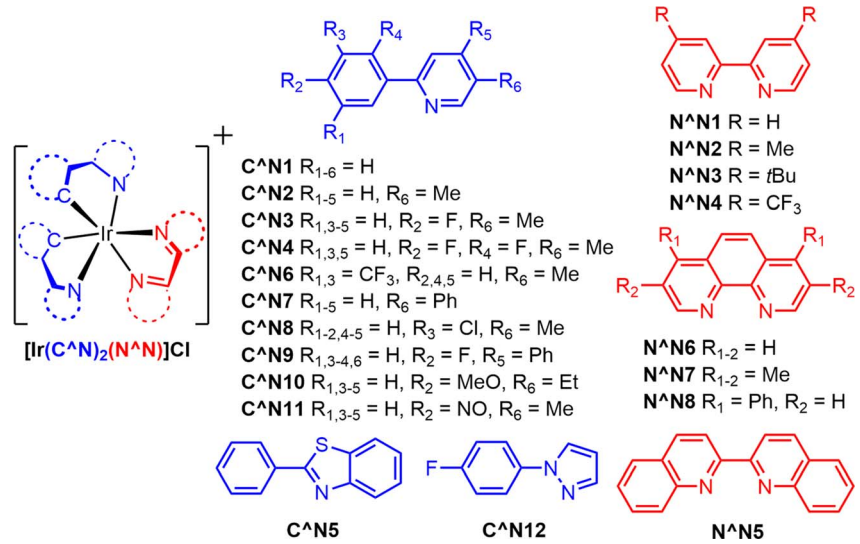

Fig. 9 Structures of photocatalysts used in experiment 2. Each complex contains two cyclometallating C^N ligands and one ancillary N^N ligand. All complexes have a Cl^- counterion.

and scarce, efforts are being made to incorporate more earth abundant materials and increase efficiency of these catalysts *via* the incorporation of inexpensive and available first row transition metals. Experiment 3 explores bimetallic water reduction catalysts for light-driven H_2 evolution with the objective of demonstrating the use of colorimetric H_2 detection films as a tool for rapidly detecting and quantifying synergistic behavior in the efficiency of the WRCs particles.

Conditions for these experiments were taken from a previous publication[31] that explored synergistic behavior of bimetallic WRCs using an iridium photosensitizer and sacrificial electron donor. The PC used for this set of experiments was $Ir(fmppy)_2(dtbbpy)PF_6$ (where fmppy = 4′-fluoro-2-phenyl-5-methylpyridine, and dtbbpy = 4,4′-di-*tert*-butyl-2,2′-bipyridine, synthesized according to literature[39]) synthesis of the PC starts with iridium(III) chloride hydrate and 2.1 mol equiv. of fmppy in a 5 : 1 ratio of 2-methoxyethanol:water and refluxed overnight. This generated a chloro-bridged iridium dimer that was precipitated with water, filtered, and dried. The resulting dimer was dissolved in a small amount of propylene glycol with 2.1 mol equiv. of dtbbpy and refluxed overnight. The crude material was diluted with water, extracted with ether, salt swapped with KPF_6, filtered, and recrystallized with acetonitrile/ether using vapor diffusion. For the HER, TEOA was used as the D, and varying amounts of nickel(II) chloride, tin(II) chloride, and potassium tetrachloropalladate were used as the salt precursors for the *in situ* generated WRCs. Stock solutions of PC and the metal salts were made in DMSO (dimethyl sulfoxide) and a TEOA 60% (w/w) solution was made in DI (deionized) water. Each sample was composed of 0.8 mL of the aqueous TEOA solution and 7.2 mL of DMSO containing 0.25 mM PC and metal salt solutions all with a total concentration of 0.2 mM. Nine different metal compositions were explored including Pd, Ni, and Sn monometallic samples in addition to PdSn and PdNi bimetallic compositions in the ratios of 1 : 0.33, 1 : 1, and 1 : 3. Samples were illuminated for 1000 minutes with pictures being taken every ten minutes.

2.4.4 Experiment 4: green hydrogen evolution. Experiments 1, 2, and 3 rely on the use of tertiary amines as electron donors, but more recent efforts are focused on the use of biomass as green donors for H_2 evolving systems. Experiment 4 surveys the chemical space of eight different hydroxyl functionalized, bio-derived species as donors on a multiwell plate to explore their capacity for H_2 production. The reaction is thought to proceed *via* an oxidative quenching pathway previously discussed.

Experimental conditions were taken from previously published work[40] that explored the use of oxalic acid, isopropanol, ethanol, and glycerol as electron donors for light driven H_2 evolution. $Ir(SCN)_2(bpy)PF_6$ (where SCN = 2-phenylbenzothiazole, and bpy = 2,2′-bipyridine, synthesized according to literature[39]) was used as the PC. Synthesis of the PC starts with iridium(III) chloride hydrate and 2.1 mol equiv. of SCN in a 5 : 1 ratio of 2-methoxyethanol and water and refluxed overnight. This generated a chloro-bridged iridium dimer that was precipitated with water, filtered, and dried. The resulting dimer was dissolved in a small amount of propylene glycol with 2.1 mol equiv. of bpy and refluxed overnight. The crude material was diluted with water, extracted with ether, salt swapped with KPF_6, filtered, and recrystallized with acetonitrile/ether using vapor diffusion. Potassium tetrachloropalladate was used as the salt precursor for the WRC and AOC, and poly(ethylene glycol) methyl ether thiol (PEG-SH, M_W = 1 kDa) served as a capping agent for the *in situ* generated nanoparticulate species. 5,5′-dimethyl propyl diquat was used as the RS and was synthesized according to literature procedures.[17] Synthesis of the RS involved the addition of 1 g of 5,5′-dimethyl-2 2′-bipyridine to 5 mL of 1,3-dibromopropane, refluxed overnight at 125 °C, filtered, and washed with ether. Eight different potentially plant-derived reagents containing hydroxyl group(s) were surveyed as electron donors including oxalic acid, isopropanol, ethanol, benzyl alcohol, glycerol, glucose, fructose, and sucrose. Stock solutions of the palladium salt and PC were made in DMSO and PEG-SH, redox shuttle, and donors were all made in

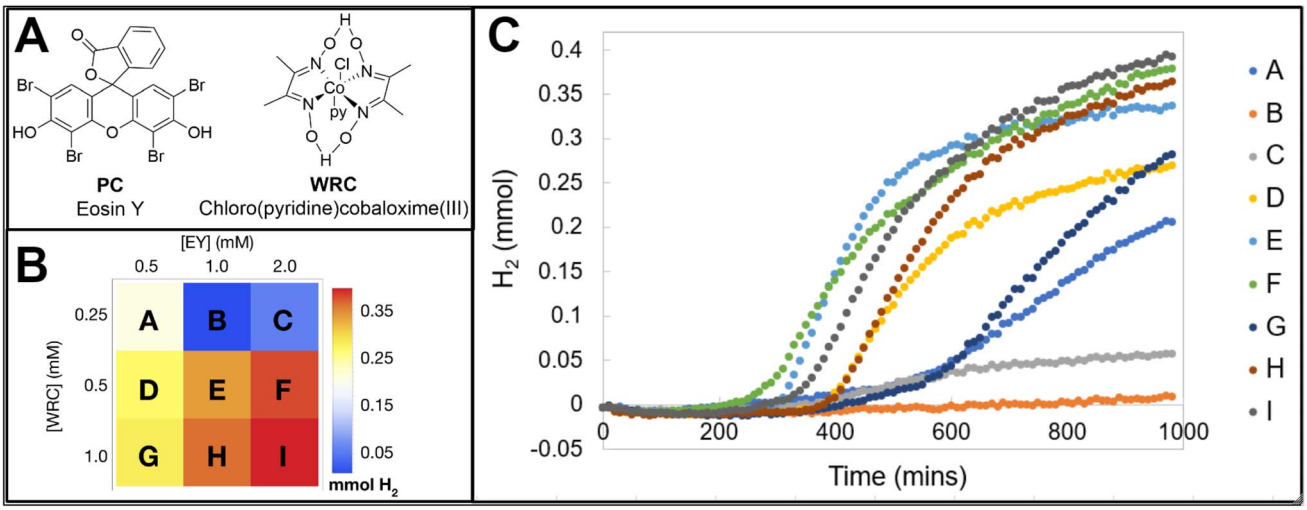

Fig. 10 (A) Structures of the PC and WRC used in experiment 1. (B) Array plot of the maximum H_2 evolved and reaction conditions for all samples in experiment 1. (C) H_2 evolution traces for experiment 1.

DI water. Each sample consisted of 225 μL of DMSO and 175 μL of water with 0.5–1.5 mM PC, 1.5 mM Pd, 1.5 mM PEG-SH, and 2–8 mM RS. Isopropanol, ethanol, and benzyl alcohol were used at 2.6 M; glycerol, fructose, sucrose, and glucose were used at 1.25 M, and oxalic acid was used at 0.52 M due to limited solubility. Samples were illuminated for 4000 minutes and pictures were taken every 30 minutes.

3 Results and discussion

3.1 Experiment 1: organic dyes and earth abundant water reduction catalysts

Due to the wealth of data provided by the image analysis software, changes in the concentration of Eosin Y and cobalt complex (structures provided in Fig. 10A) and their impact on the overall

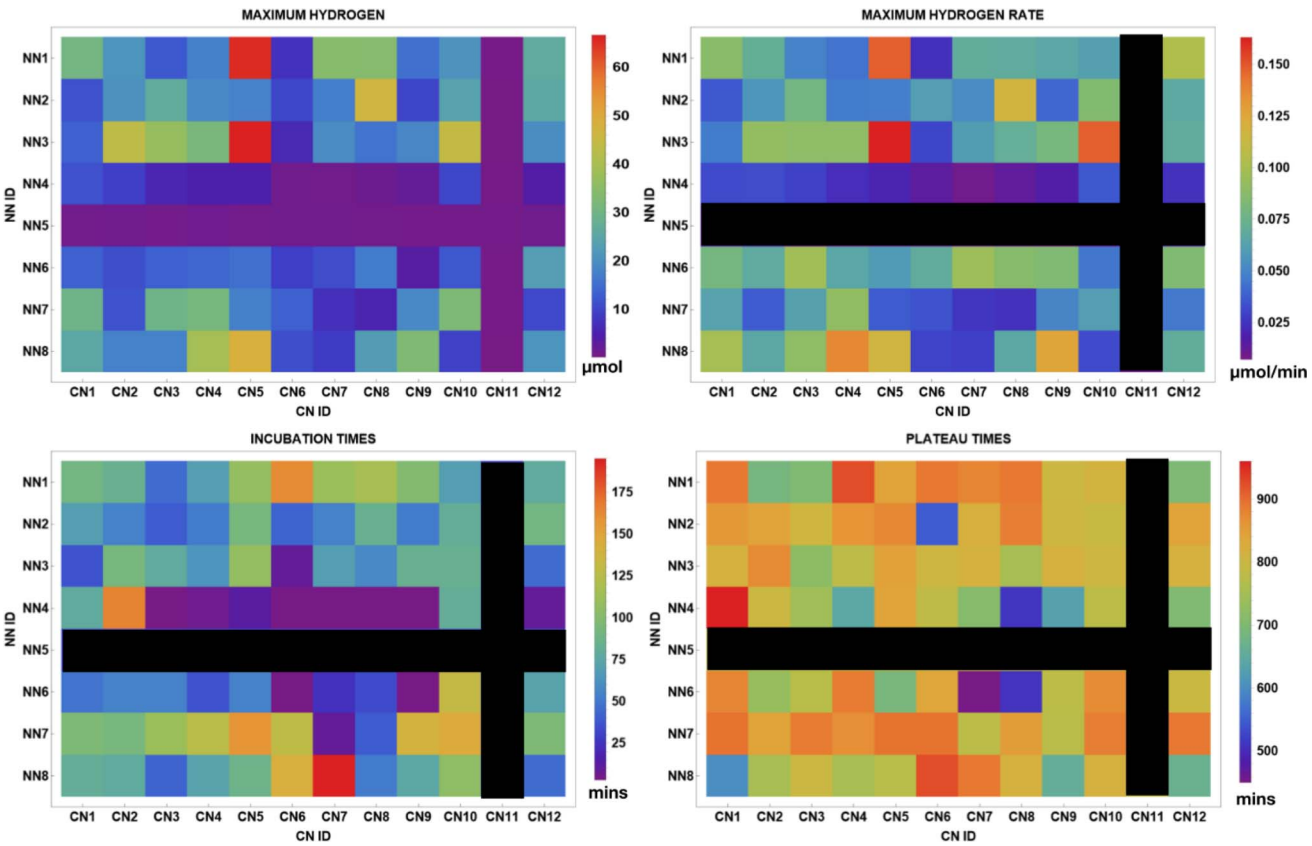

Fig. 11 Array plots displaying the total H_2 evolved, maximum H_2 rate, incubation time, and plateau times for 96 structurally unique iridium photosensitizers used in Experiment 2.

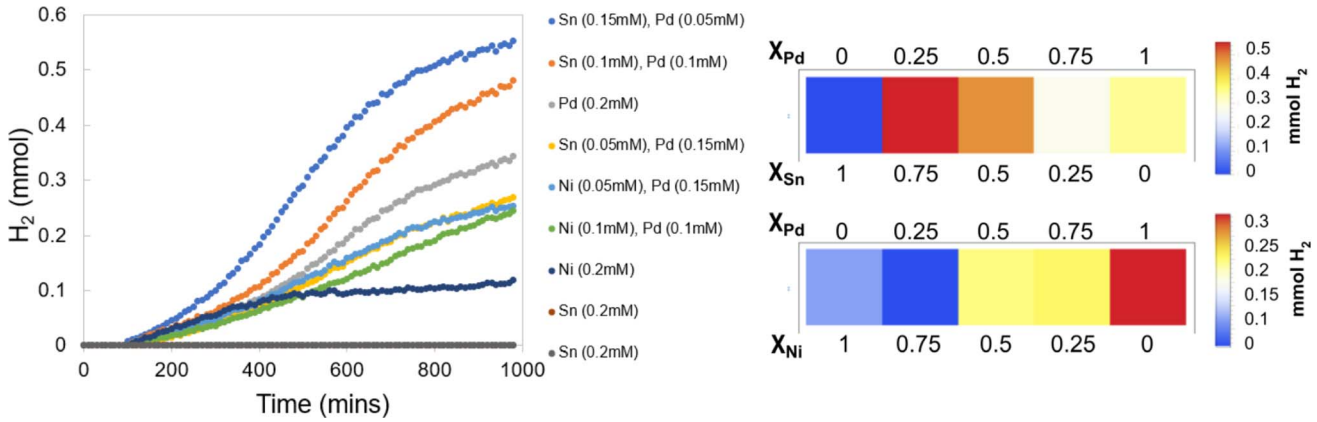

Fig. 12 H_2 evolution traces for experiment 3 (left), and array plots of overall H_2 evolution at different metal incorporations (right).

hydrogen production, rates of hydrogen production, incubation period, and plateau time can be studied. The reaction conditions and their overall hydrogen activity is shown as an array plot in Fig. 10B and the hydrogen evolution traces of the samples are shown in Fig. 10C. Generally, it is observed that increases in both the PC and WRC lead to higher amounts of hydrogen evolved. Higher concentrations of the photocatalyst yield faster onsets of hydrogen production and longer periods of activity before a plateau is observed. However, the increase in overall hydrogen production between 1 mM and 2 mM [PC] is not that significant, indicating the system may be limited by the amount of light the chromophore can absorb. When the WRC concentration is 0.5 mM, the faster rates and onsets of hydrogen production are exhibited and there is minimal improvement in overall hydrogen production between 0.5 and 1 mM. These findings are similar to what has been previously reported in the literature.

3.2 Experiment 2: structure–activity relationships with 96 unique photocatalysts

Fig. 11 displays several metrics provided from the data analysis software including the maximum H_2 produced, maximum H_2 rate, incubation time, and plateau time for each of the 96 photocatalysts. Top performing PCs for H_2 production and rate are **C^N5N^N1** and **C^N5N^N3**. No activity is present for complexes in the **C^N11** column or in the **N^N5** row. For the samples that evolved H_2, incubation times occurred under 200 minutes and plateau times ranged from about 500 minutes to 960 minutes. This data may potentially couple well with high-throughput UV-vis and luminescence spectroscopy experiments or DFT (density functional theory) calculations of the photocatalysts screened in order to further investigate how different photophysical and electronic properties impact H_2 evolution.

3.3 Experiment 3: mono and bimetallic water reduction catalysts

The colorimetric films accurately and rapidly detect the formed H_2, which allows for the identification of synergistic behavior effortlessly. Fig. 12 provides the H_2 evolution traces of the samples in addition to array plots that allow for ease in displaying the trends in metal incorporation and H_2 output. For the monometallic species, Pd affords a great deal of H_2, Ni makes a minimal amount, and Sn is completely inactive. In the Sn/Pd solutions, there is an increase in the H_2 production as the ratio of Sn : Pd increases and both the 1 : 1 and 3 : 1 samples exhibit synergistic behavior. The Ni/Pd combinations show an increase in H_2 evolution compared to the Ni only sample with lower Ni : Pd ratios leading to higher activity; however, no cases of synergy are observed.

3.4 Experiment 4: green hydrogen evolution

In this experiment, trends in RS and PC concentration on H_2 evolution for each donor can be observed. An array plot showing the total H_2 evolved in each well is shown in Fig. 13, all additional raw data points for the experiment can be found in the ESI.† Samples with donors that are easier to oxidize such as oxalic acid, benzyl alcohol, and isopropanol samples exhibit the shortest incubation times and larger amounts of H_2 evolution. Additionally, species containing more viscous and harder to oxidize donors like glycerol and fructose did not afford much H_2 and evolved the gas at slower rates.

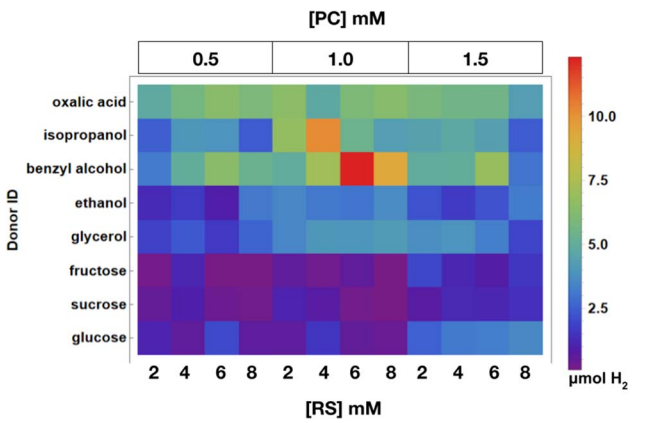

Fig. 13 Array plot displaying the total H_2 evolved for eight different donor species at three different photocatalyst concentrations and four different RS concentrations. Substrates that are easier to oxidize exhibit a quicker onset of hydrogen production and generally produce higher yields of photogenerated H_2.

4 Conclusions

In this work, colorimetric H_2 detection films are presented as a cost effective, high-throughput approach for the investigation of photo-driven (HERs). While there is great versatility in how the films can be used, HERs were monitored using a sample configuration containing a reaction vessel that houses nine vials illuminated by blue LEDs, white analysis LEDs, a stir plate, and a camera. Additionally, two experiments were conducted using the films on a multiwell plate using a photoreactor from previous work.[27] Images of the films were taken at desired time intervals over the course of a reaction using a RaspberryPi. Data analysis for calibrations and light-driven experiments were performed using a Python script that reports the RGB values of the sample wells for every picture. Two highly linear and accurate calibration methods that correlate the normalized darkness of the films to a mole fraction of hydrogen are presented. Four experiments were conducted to illustrate potential research. These experiments use earth abundant materials as photocatalysts, explore structure–activity relationships of PCs and hydrogen production, investigate the synergy in bimetallic water reduction catalysts, and study the photogeneration of green hydrogen from bioavailable donors.

Data availability

The code and analysis scripts along with processed example data supporting this article have been uploaded as part of the ESI.† This section contains a labeled image of the RaspberryPi and relay board wiring configuration for the 20 mL vial photoreactor and the calibration curve used for the analysis of the multi-well plate experiments (PDF). It also includes the processed image analysis data and a movie of the reaction progress from Experiment 2, information on making a mask, image analysis Python script, photoreactor Python script, and sample holder STL file for 3D printing (ZIP files).

Author contributions

Savannah Talledo: conceptualization, data curation, formal analysis, investigation, methodology, project administration, resources, visualization, writing – original draft, writing – review & editing. Andrew Kubaney: resources, software, writing – review and editing. Mitchell A. Baumer: resources, visualization, writing – review and editing. Keegan Pietrak: resources. Stefan Bernhard: conceptualization, project administration, writing – review & editing.

Conflicts of interest

There are no conflicts to declare.

Acknowledgements

We are grateful for the financial support from the US National Science Foundation (CHE-2102460).

References

1 P. Sun, B. Young, A. Elgowainy, Z. Lu, M. Wang, B. Morelli and T. Hawkins, *Environ. Sci. Technol.*, 2019, **53**, 7103–7113.
2 G. Collodi and F. Wheeler, *Chem. Eng. Trans.*, 2010, **19**, 37–42.
3 S. P. Luo, E. Mejía, A. Friedrich, A. Pazidis, H. Junge, A. E. Surkus, R. Jackstell, S. Denurra, S. Gladiali, S. Lochbrunner and M. Beller, *Angew. Chem., Int. Ed.*, 2013, **52**, 419–423.
4 H. Lv, J. Song, H. Zhu, Y. G. Geletii, J. Bacsa, C. Zhao, T. Lian, D. G. Musaev and C. L. Hill, *J. Catal.*, 2013, **307**, 48–54.
5 C. Bachmann, B. Probst, M. Oberholzer, T. Fox and R. Alberto, *Chem. Sci.*, 2016, **7**, 436–445.
6 I. Tabushi and Y. Akira, *J. Org. Chem.*, 1981, **46**, 1899–1901.
7 E. H. Edwards, J. Jelušić, S. Chakraborty and K. L. Bren, *J. Inorg. Biochem.*, 2021, **217**, 111384.
8 S. F. Chan, M. Chou, C. Creutz, T. Matsubara and N. Sutin, *J. Am. Chem. Soc.*, 1981, **103**, 369–379.
9 K. Kalyanasundaram, J. Kiwi and M. Grätzel, *Helv. Chim. Acta*, 1978, **61**, 2291–2755.
10 K. A. Davis, S. Yoo, E. W. Shuler, B. D. Sherman, S. Lee and G. Leem, *Nano Convergence*, 2021, **8**, 1–19.
11 A. V. Puga, *Coord. Chem. Rev.*, 2016, **315**, 1–66.
12 H. Hata, Y. Kobayashi, V. Bojan, W. J. Youngblood and T. E. Mallouk, *Nano Lett.*, 2008, **8**, 794–799.
13 Y. Bai, C. Li, L. Liu, Y. Yamaguchi, M. Bahri, H. Yang, A. Gardner, M. A. Zwijnenburg, N. D. Browning, A. J. Cowan, A. Kudo, A. I. Cooper and S. Sprick, *Angew. Chem., Int. Ed.*, 2022, **61**, e202201299.
14 J. McFarlane, B. Henderson, S. Donnecke and J. S. McIndoe, *Organometallics*, 2019, **38**, 4051–4053.
15 M. C. Nevárez Martínez, O. Cavdar, L. P. Haliński, M. Miodyńska, P. Parnicka, B. Bajorowicz, M. Kobylański, L. Lewandowski and A. Zaleska-Medynska, *Int. J. Hydrogen Energy*, 2022, **47**, 15783–15788.
16 H. N. Kagalwala, D. N. Chirdon, I. N. Mills, N. Budwal and S. Bernhard, *Inorg. Chem.*, 2017, **56**, 10162–10171.
17 M. L. K. Sanchez, C. H. Wu, M. W. W. Adams and B. R. Dyer, *Chem. Commun.*, 2019, **55**, 5579–5582.
18 A. A. Nada, M. H. Barakat, H. A. Hamed, N. R. Mohamed and T. N. Veziroglu, *Int. J. Hydrogen Energy*, 2005, **30**, 687–691.
19 V. Kumaravel, M. D. Imam, A. Badreldin, R. K. Chava, J. Y. Do, M. Kang and A. Abdel-Wahab, *Catalysts*, 2019, **9**, 276.
20 H. Dong, J. Li, M. Chen, H. Wang, X. Jiang, Y. Xiao, B. Tian and X. Zhang, *Materials*, 2019, **12**, 2233.
21 Y. Bai, L. Wilbraham, B. J. Slater, M. A. Zwijnenburg, R. S. Sprick and A. I. Cooper, *J. Am. Chem. Soc.*, 2019, **141**, 9063–9071.
22 B. D. Adams and A. Chen, *Mater. Today*, 2011, **14**, 282–289.
23 Y. Cui, F. Liang, C. Ji, S. Xu, H. Wang, Z. Lin and J. Liu, *ACS Omega*, 2019, **4**, 7428–7435.
24 L. Chen, A. C. Cooper, G. P. Pez and H. Cheng, *J. Phys. Chem. C*, 2007, **111**, 18995–19000.

25 V. Bérubé, G. Radtke, M. Dresselhaus and G. Chen, *Int. J. Energy Res.*, 2007, **31**, 637–663.
26 Y. Xi, Q. Zhang and H. Cheng, *J. Phys. Chem. C*, 2014, **118**(1), 494–501.
27 E. M. Lopato and S. Bernhard, *Energy Fuels*, 2021, **35**, 18957–18981.
28 A. V. Vorontsov, I. V. Stoyanova, D. V. Kozlov, V. I. Simagina and E. N. Savinov, *J. Catal.*, 2000, **189**, 360–369.
29 Z. He, L. Xie, J. Tu, S. Song, W. Liu, Z. Liu, J. Fan, Q. Liu and J. Chen, *J. Phys. Chem. C*, 2010, **114**, 526–532.
30 Z. W. Abdullah and Y. Dong, *Front. Mater.*, 2019, **6**, 58.
31 E. M. Lopato, E. A. Eikey, Z. C. Simon, S. Back, K. Tran, J. Lewis, J. F. Kowalewski, S. Yazdi, J. R. Kitchin, Z. W. Ulissi, J. E. Millstone and S. Bernhard, *ACS Catal.*, 2020, **10**, 4244–4252.
32 M. Majek, F. Filace and A. J. von Wangelin, *Beilstein J. Org. Chem.*, 2014, **10**, 981–989.
33 M. Majek and A. J. von Wangelin, *Acc. Chem. Res.*, 2016, **49**, 2316–2327.
34 M. Wang, Y. Na, M. Gorlov and L. Sun, *Dalton Trans.*, 2009, **33**, 6458–6467.
35 P. Du and R. Eisenberg, *Energy Environ. Sci.*, 2012, **5**, 6012–6021.
36 R. N. Motz, E. M. Lopato, T. U. Connell and S. Bernhard, *Inorg. Chem.*, 2021, **60**, 774–781.
37 D. L. Jameson, J. J. Grzybowski, D. E. Hammels, R. K. Castellano, M. E. Hoke, K. Freed, S. Basquill, A. Mendel and W. J. Shoemaker, *J. Chem. Educ.*, 1998, **75**, 447–450.
38 V. Mdluli, S. Diluzio, J. Lewis, J. F. Kowalewski, T. U. Connell, D. Yaron, T. Kowalewski and S. Bernhard, *ACS Catal.*, 2020, **10**, 6977–6987.
39 L. T. Tinker, N. D. McDaniel, E. D. Cline, S. Bernhard, R. D. Putnam and T. B. Rauchfuss, *Inorg. Synth.*, 2010, **35**, 168–173.
40 E. M. Lopato, S. Talledo, S. Diluzio, V. Mdluli, Z. C. Simon, K. M. McHugh, J. E. Millstone and S. Bernhard, *ACS Sustainable Chem. Eng.*, 2022, **10**, 14248–14261.